Negative Differential Conductance Induced by Majorana Bound States Side-Coupled to T-Shaped Double Quantum Dots

Yu Mei Gao , Yi Fei Huang * , Feng Chi * , Zichuan Yi , Liming Liu

Posted Date: 23 June 2025

doi: 10.20944/preprints202506.1820.v1

Keywords: electronic transport; negative differential conductance; double quantum dots; Majorana bound states; zero-bias anomaly

Article

Negative Differential Conductance Induced by Majorana Bound States Side-Coupled to T-Shaped Double Quantum Dots

Yu-Mei Gao[1], Yi-Fei Huang[2*],Feng Chi[1,†] Zi-Chuan Yi[1], and Li-Ming Liu[1]

[1] School of Electronic and Information Engineering, UEST of China, Zhongshan Institute, Zhongshan 528400, China
[2] School of General Education, Quanzhou Ocean Vocational College, Quanzhou 362700, China
* Correspondences: huangyifei2020@126.com or chifeng@semi.ac.cn

Abstract: Electronic transport through T-shaped double quantum dots (TDQDs) connected to normal metallic leads is studied theoretically by using the nonequilibrium Green's function method. It is assumed that the Coulomb interaction exists only in the central QD (QD-1) that directly coupled to the leads, and is absent in the other reference QD (QD-2) side-coupled to QD-1. We also consider the impacts of Majorana bound states (MBSs), which are prepared at the opposite ends of a topological superconductor nanowire (Majorana nanowire) hybridized to QD-2, on the electrical current and differential conductance. Our results show that by the combined effects of the Coulomb interaction in QD-1 and the MBSs, a phenomenon of negative differential conductance (NDC) emerges near the zero-bias point. Now the electrical current decreases despite of increasing bias voltage. The NDC is prone to occur under the conditions of low temperature and both of the two QDs' energy levels are in resonant to the zero Fermi level. Its magnitude characterized by a peak-to-valley ratio can be enhanced up to 3 by increasing the interdot coupling strength, and depends on the dot-MBS hybridization strength nonlinearly. This prominent NDC combined with the previously found zero-bias anomaly (ZBA) of the differential conductance are useful in designing novel quantum electric devices, and may also serve as an effective detection means for the existence of MBSs which is still a challenge in solid-state physics.

Keywords: electronic transport; negative differential conductance; double quantum dots; Majorana bound states; zero-bias anomaly

1. Introduction

Majorana bound states (MBSs) are zero-energy quasiparticle states that were early predicted to appear in topological superconductors at boundaries or in vortices[1–3]. These localized excitations are their own antiparticles which means that they are neither bosons nor fermions, but are topologically protected objects called "non-Abelian anyons". They are then immune to all local perturbations and are protected by the topological gap itself. This makes them to be a potential candidate in constructing qubits for fault-tolerant topological quantum computer[4,5]. The MBSs were early observed experimentally in a semiconductor-superconductor nanowire (Majorana nanowire) with strong spin-orbit interaction under a magnetic field manifested as zero bias conductance peak (ZBCP)[6,7] or fractional Josephson effect[8]. There are also some other solid-state platforms for creating MBSs such as coupling conventional superconductor to topological insulator[9,10] or conventional semiconductor[11], doped topological insulators[12], iron-based superconductors[13], quantum Hall analogs of spinless superconductors[14], superconducting topological crystalline insulator[15], superconducting shell surrounding a spin-orbit-coupled semiconducting nanowire core[16]. A recent work proposed to generate MBSs in superconductor/topological-insulator/superconductor hybrid system under very weak magnetic field[17], which is fundamentally different from previous work relying on strong magnetic field.

 doi:10.20944/preprints202506.1820.v1

Currently, detecting MBSs remains challenging as localized non-topological states can mimic their signatures. Much theoretical and experimental work have been carried out to probe the signatures of MBSs through phenomena including the 4π periodic Josephson current-phase in junctions between topological superconductors[18], half-integer conductance plateau at the coercive field in a hybrid structure composing of topological superconductors and topological quantum anomalous Hall insulator[19], enhancement or sign inversion of the thermopower in thermoelectricity[20–24], interaction between MBSs and microwave[25–29], and ZBCP at the edges of the Majorana nanowires[6,7]. Among the above detection schemes for MBSs, ZBCP in electrical transport measurements is the most popular one. But ZBCP can also be induced by other mechanisms, and was classified by Pan and Das Sarma as: good (by actual MBSs), bad (by Andreev Bound states which maybe called quasi-MBSs, produced by accidental quantum dots (QDs) in the nanowire), and ugly (by random disorder) ones[30]. Therefore, researchers have been continuously putting forward other powerful approaches to verify the existence of MBSs, of which hybrid setups with MBSs side-coupled to QDs are attractive. QDs are zero-dimensional mesoscopic device with adjustable energy levels, electron-electron Coulomb interactions, particle numbers and coupling strength to external environment[31]. In a system composing of MBSs side-coupled to a QD, Liu predicted theoretically a half-maximum conductance, which originate from the half-fermionic nature of the MBSs, emerges when the QD's energy level is aligned to the electrochemical potentials of the leads connected to the QD[32]. This is a reliable evidence of the MBSs and has subsequently been observed in experiment with a QD coupled to an InAs-Al nanowire[33].

Distinguishing MBSs through differential tunneling conductance spectroscopy in hybridized QDs-MBSs system has been under intensive investigation in recent years[34–37]. Some works were also devoted to identify the MBSs by combing electrical transport measurements with quantum interference effects in multiple-QD or multiple-path systems[38–43]. In such systems, both the peak's height and positions of the differential conductance are varied by the coaction of MBSs and interference effects, and then maybe used for detecting the existence of MBSs or for preparing other functional electrical devices. In the present paper, we study electronic transport through a T-shaped double QDs (TDQDs) in the presence of MBSs, see the schematic plot in Figure 1 in which QD-1 is coupled to two normal metallic leads and to QD-2, which is further side-coupled to one mode of the MBSs prepared at the ends of a Majorana nanowire. Especially, we focus on the phenomenon of negative differential conductance (NDC) induced by the MBSs and interference effect. The NDC refers to a decrease in current with increasing bias voltage, and is unique in mesoscopic systems[44–49]. It has attracted much interest in view of its wide applications in designing various electronic devices, including logic circuits, fast switching, low-power memory, and various energy-saving devices[43]. The NDC has been observed in many devices such as molecules[46,47], monolayers[48], and systems based on semiconductor quantum dots (QDs)[44,45,49]. Physical origins of the NDC effect may be attributed to features of the electrodes or the interface, bias-dependent tunnel-barriers, spin or phonon blockade, conformational switching, and quantum interferences[43], etc. Currently, applications of NDC are hindered by two factors. One is the relatively small magnitude with a peak-to valley ratio less than 2, and the other is the exhibition in relatively high bias region that will consume more energy. Here we find that the NDC generally occurs near zero-bias point, and the peak-to-valley ratio can reach as large as about 3 when the central QD-1 is coupled weakly to the leads and strongly to QD-2, and thus will be helpful to overcome the above two hinderments.

 doi:10.20944/preprints202506.1820.v1

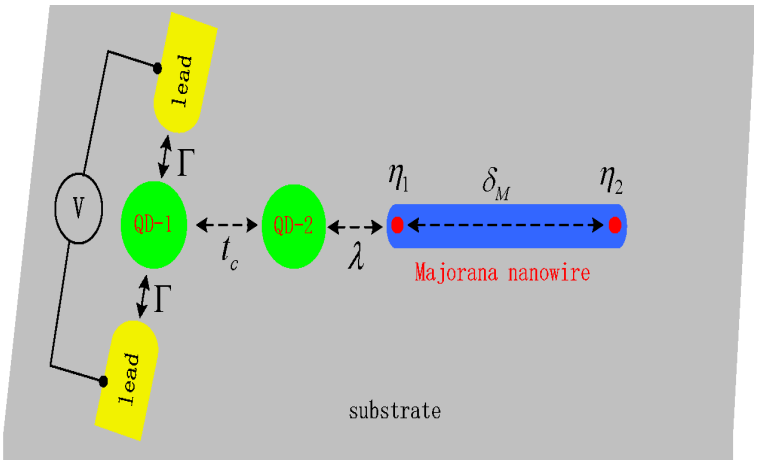

Figure 1. Schematic setup of T-shaped double quantum dots of which dot-1 is connected to the upper and lower metallic leads with equal strengthes Γ, and tunnel couples to dot-2 with strength t_c. QD-2 is also side-coupled to a Majorana nanowire hosting MBSs (red circles at the ends of the nanowire), which are denoted individually by γ_1 and γ_2. The mode η_1 couples to QD-2 with strength of λ, and to mode η_2 with strength of δ_M.

2. Model and Method

The Hamiltonian of the present studied system can be written in the following form[32,38,50]

$$H = \sum_{k\alpha\sigma} \varepsilon_{k\alpha\sigma} c^{\dagger}_{k\alpha\sigma} c_{k\alpha\sigma} + \sum_{i=1,2;\sigma} \varepsilon_i d^{\dagger}_{i\sigma} d_{i\sigma} + U d^{\dagger}_{1\uparrow} d_{1\uparrow} d^{\dagger}_{1\downarrow} d_{1\downarrow} + \sum_{k\alpha\sigma} (V_{k\alpha} c^{\dagger}_{k\alpha\sigma} d_{1\sigma} + H.c) + H_{MBSs}, \tag{1}$$

where $c^{\dagger}_{k\alpha\sigma}$ ($c_{k\alpha\sigma}$) creates (annihilates) an electron of momentum k, energy $\varepsilon_{k\alpha\sigma}$, and spin direction of $\sigma = \uparrow, \downarrow$ in the upper and lower leads ($\alpha = U, L$). The operator $d^{\dagger}_{i\sigma}$ ($d_{i\sigma}$) is the creation (annihilation) operator of an electron in dot-i with gate voltage tunable energy level ε_i, spin-σ. We assume that there is intradot Coulomb interaction U only in QD-1. The coupling strength between QD-1 and lead$-\alpha$ is described by $V_{k\alpha}$. The last term H_{MBSs} in Eq. (1) is for the MBSs prepared at opposite ends of the Majorana wire[32,38,51]. Here we consider the case that only one mode of the MBSs couples to the spin-up electrons in QD-2 due to the helical nature of the MBSs[32,38,51]. The hybridization strength between QD-2 and MBS is denoted by λ, and the explicit expression of H_{MBSs} is[32,38,51],

$$H_{MBSs} = i\delta_M \eta_1 \eta_2 + \lambda (d_{2\uparrow} - d^{\dagger}_{2\uparrow}) \eta_1, \tag{2}$$

in which δ_M is the interaction strength between the MBSs whose operators satisfy $\eta_i = \eta^{\dagger}_i (i = 1, 2)$ and $\{\eta_i, \eta_j\} = 2\delta_{i,j}$. As usual, we rewrite η_j in terms of the regular fermionic operators f as $\eta_1 = (f^{\dagger} + f)/\sqrt{2}$ and $\eta_2 = i(f^{\dagger} - f)/\sqrt{2}$, and then H_{MBSs} is given by[32,38,51]

$$\tilde{H}_{MBSs} = \delta_M (f^{\dagger} f - \frac{1}{2}) + \frac{\lambda}{\sqrt{2}} (d_{2\uparrow} - d^{\dagger}_{2\uparrow})(f^{\dagger} + f). \tag{3}$$

The spin-dependent current J_σ tunneling between QD-1 and the leads is calculated in terms of the nonequilibrium Green's function technique[32,38]

$$J_\sigma = \frac{e}{h} \int \frac{d\varepsilon}{2\pi} \frac{\Gamma_U \Gamma_L}{\Gamma_U + \Gamma_L} [-2\mathrm{Im} G^r_{1\sigma}(\varepsilon)][f_U(\varepsilon) - f_L(\varepsilon)], \tag{4}$$

where the line-width function $\Gamma\alpha = 2\pi |V_{k\alpha}|^2 \rho_\alpha$ and ρ_α being the local density of states of electrons in lead$-\alpha$. Under the wide-band approximation, we set $\rho_\alpha \equiv 1$ in the following numerical calculations. The quantity $f_\alpha(\varepsilon) = 1/\{1 + \exp[(\varepsilon - \mu_\alpha)/k_B T]\}$ is the Fermi-Dirac distribution function in lead$-\alpha$ with chemical potential μ_α, temperature T and Boltzmann constant k_B, respectively. The term $-2\mathrm{Im} G^r_{1\sigma}(\varepsilon)$ in the above equation means the imaginary part of the retarded Green's function of

 doi:10.20944/preprints202506.1820.v1

QD-1, which is obtained by adopting the equation of motion method. Its explicit expression is give by[21,22,38,51,52],

$$G^r_{1\sigma} = \frac{\varepsilon_{1U} + U < n_{1\bar{\sigma}} >}{\varepsilon_{1U}[\varepsilon_{1-} - \Pi_\sigma(\varepsilon)]}, \tag{5}$$

in which $\varepsilon_{1U} = \varepsilon_{1-} - U - t_c^2/(\varepsilon - \varepsilon_2 + i0^+)$, and

$$\Pi_\sigma = \frac{t_c^2(\varepsilon_{2+}\varepsilon_{1+} - t_c^2)}{\varepsilon_{2-}(\varepsilon_{2+}\varepsilon_{1+} - t_c^2) - \varepsilon_{1+}K^2}, \tag{6}$$

where $\varepsilon_{i\pm} = \varepsilon \pm \varepsilon_i + i(\Gamma_U + \Gamma_L)/2$ and $K = 2\varepsilon/(\varepsilon^2 - \delta_M^2 + i0^+)$. The electron occupation number $< n_{1\sigma} >$ in Eq. (5) needs to be calculated self-consistently from the following equation[21,22,53],

$$< n_{1\sigma} >= \int d\varepsilon \frac{\Gamma_U f_U(\varepsilon) + \Gamma_L f_L(\varepsilon)}{\Gamma_U + \Gamma_L}[-\mathrm{Im}G^r_{1\sigma}(\varepsilon)/\pi]. \tag{7}$$

3. Numerical Results

In numerical calculations, we set the intradot Coulomb interaction $U = 1$ as the energy unit, and consider that QD-1 couples to the upper and lower leads with equal strengths $\Gamma_U = \Gamma_L = \Gamma$. Figure 2 presents the electrical current J_σ and the corresponding differential conductance $G_\sigma = dJ_\sigma/dV$ varying with the applied bias voltage bias in the absence of the Coulomb interaction ($U = 0$). Under these conditions, our results are essentially in consistent with those of Gong *et al*[38]. For $\lambda = 0$, the electrical current $J_\uparrow = J_\downarrow$ increases whenever the chemical potentials of the leads $\mu_U = -\mu_L = eV/2$ is aligned to the molecular states $\varepsilon = \pm t_c$ for the dots' levels $\varepsilon_1 = \varepsilon_2 = 0$, which is indicated by the red dashed line in Figure 2(a). Correspondingly, the differential conductance develops peaks at $eV = \pm 2t_c$ as shown by the black solid line in Figure 2(a)[38,49,50,53]. We next show the spin-up conductance $G_\uparrow$ in Figure 2(b) when QD-2 interacts to the MBS prepared at the end of Majorana wire ($\lambda \neq 0$). The spin-down conductance is the same as in Figure 2(a) in the case of $U = 0$. Figure 2(b) shows that the peaks in $G_\uparrow$ originally positioned at $\pm 2t_c$ are suppressed and then split for large enough λ as indicated by the blue dotted and purple dash-dotted lines. More interestingly, a new peak emerges at zero-bias point ($V = 0$) which is the previously found zero-bias abnormality (ZBA) induced by MBSs[32,38,51]. The peak's height of $G_\uparrow|_{V=0}$ is exactly equal to $e^2/(2h)$, which shows the half-fermion nature of the MBSs. This result agrees with those found in either single QD[32] or TDQDs[38] structures in the presence of MBSs. Since the height of the ZBA is completely unaffected by the value of MBS-QD hybridization strength, it can be viewed as an evidence of the existence of MBSs. If the Majorana nanowire is replaced by conventional superconducting nanowire, Andreev reflection processes will also induce peak in the differential conductance around the zero-bias point[54]. The peak height in this case, however, depends on the hybridization strength between the QD and the superconductor, which is quite different from the present result. Figures 2(c) and (d) show the current J_σ and the associated differential conductance G_σ as functions of the bias voltage for fixed $\lambda = 0.1$ and different values of Γ. As usual, the current in Figure 2(c) increases whenever the bias voltage is aligned to the molecular states $\pm 2t_c$, and then G_σ develops peaks. The peaks become wider and higher with increasing value of Γ due to stronger interaction between QD-1 and the leads.

 doi:10.20944/preprints202506.1820.v1

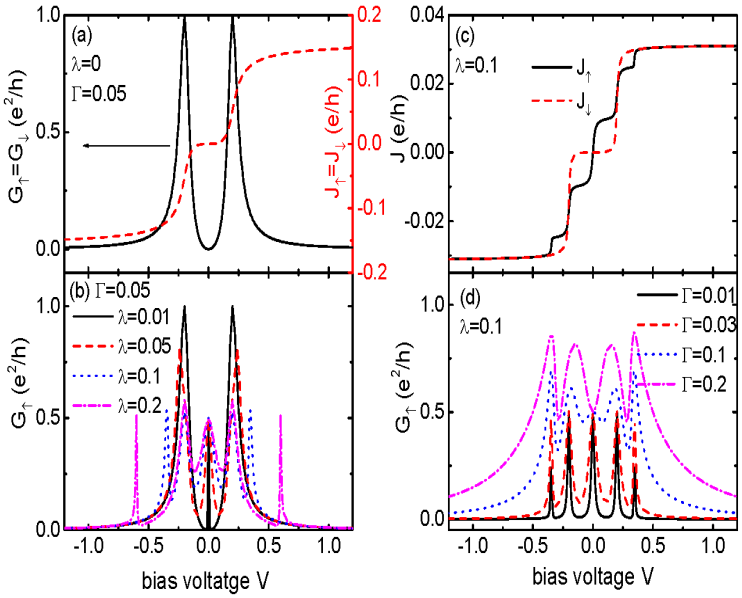

Figure 2. Spin-dependent current J_σ in (a), (c), and the corresponding differential conductance in (b), (d) varying with the bias voltage in the case of intradot Coulomb interaction $U = 0$. Now the spin-down current and differential conductance are not affected by the MBSs as only spin-up electrons in QD-2 couple to the MBS. The energy levels of the two dots are all set to be zero ($\varepsilon_1 = \varepsilon_2 = 0$), inter-dot coupling strength $t_c = 0.1$, and the system temperature $T = 0$.

In Figure 3, we present the spin-up differential conductance $G_\uparrow$ for fixed intradot Coulomb interaction $U = 1$. Under this condition, although the MBSs also affect transport processes of the spin-down electrons, the impacts are relatively weak and then $G_\downarrow$ is not shown here. If QD-2 are free from coupling to the MBS ($\lambda = 0$), the Coulomb blockade effect will induce a pair of peaks in $G_\uparrow$ around $eV = \pm 2U$, which are less affected by the MBSs and then are also not shown here. The peaks in $G_\uparrow$ at $\pm 2t_c$ previously shown in Figure 2 still survive as indicated in Figure 3(a). Different from the case of $U = 0$, another pair of peaks emerge around $eV \approx \Gamma$ due to the constructive quantum interference effect in the presence of finite Coulomb interaction in QD-1. Turning on coupling between QD-2 and the MBS ($\lambda \neq 0$), the peaks around $\pm 2t_c$ are lowered and split as those in Figure 2(b). The ZBA with fixed height of $e^2/2h$ emerges again due to the hybridization between QD-2 and the MBS. As a result of it, the original peaks around $eV \approx \pm\Gamma$ are suppressed, and can even become negative by increased λ, the interesting NDC phenomenon. The magnitude of the NDC depends nonlinearly on the value of λ. For $\lambda \sim \Gamma$, the absolute value of NDC has a maximum of $|G_\uparrow| \approx e^2/2h$, and then decreases with increasing λ.

 doi:10.20944/preprints202506.1820.v1

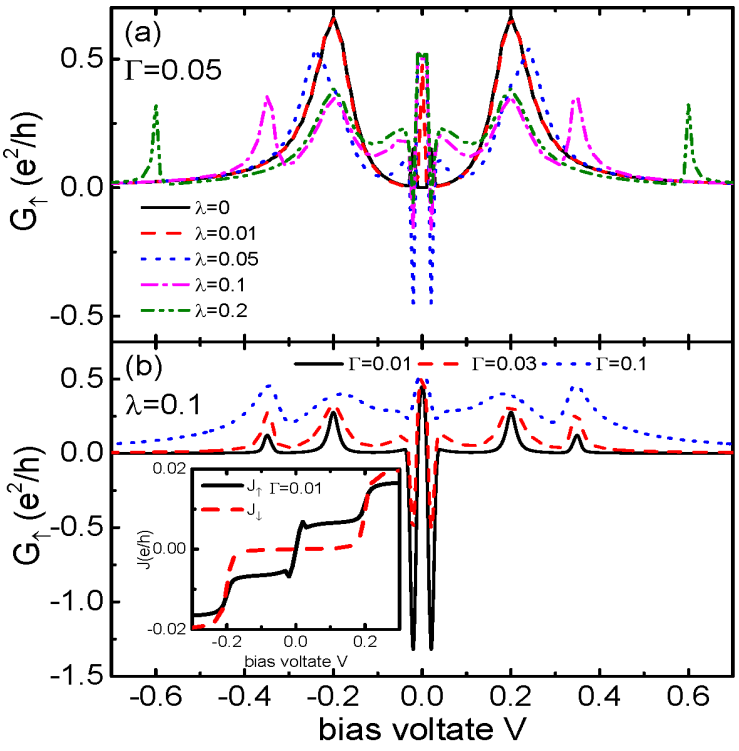

Figure 3. Spin-up differential conductance $G_\uparrow$ as a function of the bias voltage V for $U = 1$ and different λ in (a) and different Γ in (b). The inset in (b) shows the spin-resolved current varying with the bias voltage with $\lambda = 0.1$ and $\Gamma = 0.01$. The system temperature is set to be zero.

The origin of the NDC can be explained as follows[43–45]: Under the conditions of $\lambda = 0$ and $U = 0$, destructive quantum interference takes place when the energy of the electrons in QD-1 is the same as the that of electrons in the side-coupled QD-2, leading to the well-known Fano antiresonance effect[38]. In the zero-bias limit, only the zero-energy electron takes part in the quantum transport, and then the differential conductance is zero. The intradot Coulomb interaction provides another electron transport path in QD-1, and then results in constructive quantum interference around the bias voltage $eV \approx \pm\Gamma$ and arises conductance peaks as indicated by the solid black line in Figure 3(a). When QD-2 is coupled to the MBS, the newly developed ZBA indicates the original destructive quantum interference is changed into constructive one. According to the compensation principle, the previous constructive quantum interference effect around $eV \approx \pm\Gamma$ becomes to destructive one, and then the height of $G_\uparrow$ is suppressed. Due to the exotic nature of the MBSs, the value of $G_\uparrow$ can even be suppressed to negative vaue. The zero-energy conductance peak with half quantum maximum $e^2/2h$ accompanied by the NDC found in this TDQDs structure provide a strong evidence of the existence of MBSs. Figure 3(b) shows that $G_\uparrow$ is sensitive to the value of Γ. At weak coupling between the the leads and QD-1, the NDC is obviously enhanced with $G_\uparrow(eV \approx \pm\Gamma)$ can reach about $-1.25e^2/h$. This can be seen from the inset in Figure 3(b) in which $J_\uparrow$ indicated by the solid black line decreases with increasing bias voltage around $eV \approx \pm\Gamma$. The spin-down current varies smoothly at $eV \approx \pm\Gamma$. Comparing the behaviors of $J_\uparrow$ and $J_\downarrow$, the NDC can be attributed to the existence of MBSs. Increasing the value of Γ, the magnitude of NDC is weakened accompanied by the widening of other peaks. For large enough $\Gamma = 0.1$, the NDC disappears as indicated by the blue dotted line in Figure 3(b) because the functions of the MBS are suppressed when electrons are strongly coupled to the leads.

Figure 4 presents the dependence of $G_\uparrow$ and $J_\uparrow$ on the interdot coupling t_c with fixed $\lambda = 0.1$. For weak interdot coupling $t_c = 0.01$, the height of the ZBA induced by MBS is fixed at $e^2/2h$, and the other two peaks with positive values locate about at $eV = \pm t_c$. With increasing value of t_c, the peaks are lowered and split similar to the cases in Figures 2 and 3, except those of the ZBA. When the interdot coupling is strong enough, NDC emerges as is indicated by the blue dotted and purple

 doi:10.20944/preprints202506.1820.v1

dash-dotted lines in Figure 3(a). The magnitude of the NDC is enhanced by increasing t_c as the impact of MBS is strengthened. Meanwhile, it is found that the peaks at higher energy states $\varepsilon \approx \pm\sqrt{t_c^2+\lambda^2}$ are further split and become higher. This is because that the value of the original conductance peaks around $\pm\Gamma$ are changed from positive to negative inducing the phenomenon of NDC, more electrons will transport through the system from the energy states of $\pm\sqrt{t_c^2+\lambda^2}$ and result increased $G_\uparrow$. Figure 3(b) shows that the magnitude of $J_\uparrow$ is weakened by increasing t_c due to the quantum interference processes. For $t_c = 0.15$ and 0.2, it decreases with increasing bias voltage around $eV \approx \pm\Gamma$ and results in the phenomenon of NDC. As a contrast, the spin-down current $J_\downarrow$ in the inset increases obviously at the molecular states of $\pm\sqrt{t_c^2+\lambda^2}$ which leads to peaks in the differential conductance. Apart from these two states, $J_\downarrow$ changes smoothly and no peak is induced in the differential conductance.

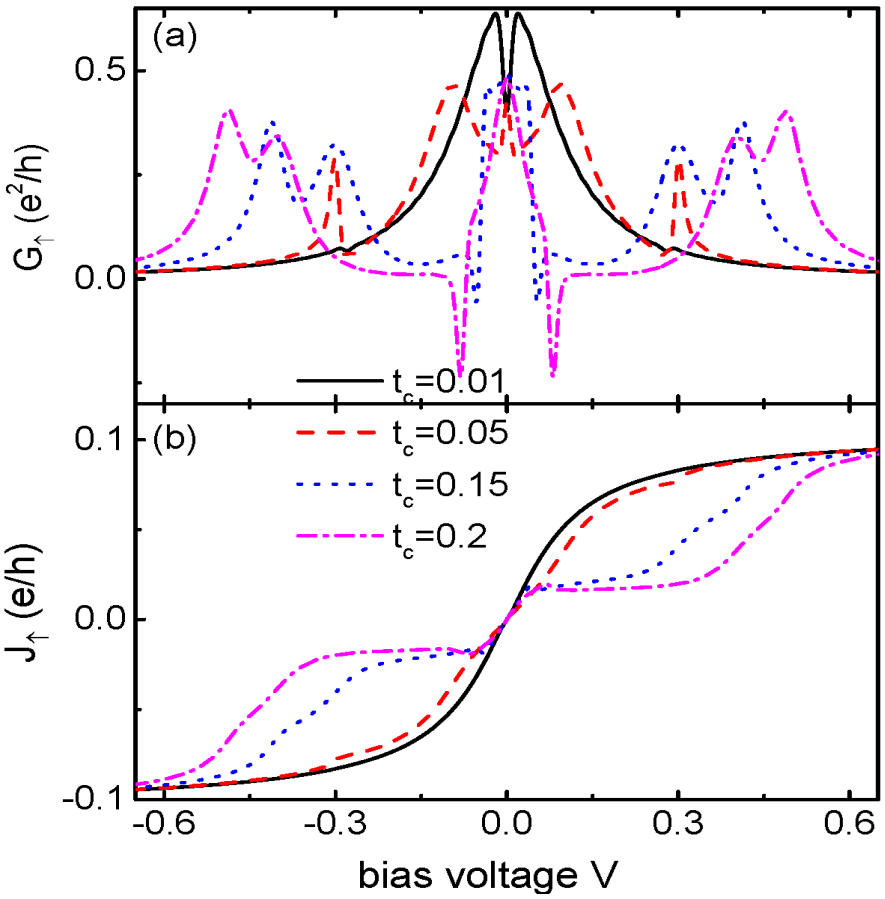

Figure 4. (a) Spin-up differential conductance $G_\uparrow$ and (b) spin-up current $J_\uparrow$ as functions of the bias voltage V for $U = 1, \Gamma = 0.05, \lambda = 0.1, T = 0$, and different values of inter-dot coupling strength t_c. The NDC is enhanced by increasing t_c.

In experiments, the energy levels of the QDs can be adjusted by external gate voltages and will change the transport processes drastically. In Figure 5, we examine the impacts of QDs' energy levels' configuration $(\varepsilon_1, \varepsilon_2)$ on the differential conductance. Figure 5(a) shows that the ZBA in $G_\uparrow$ with height of $e^2/2h$ is essentially not changed by the variation of dots' energy levels, showing the reliable evidence for the existence of MBSs. Apart from the zero-bias point, both the position and height of the conductance peaks are sensitive to the configuration of the QDs' energy levels $(\varepsilon_1, \varepsilon_2)$. Importantly, the NDC disappears when the QDs' energy levels are not aligned to the Fermi level of the leads μ as the destructive quantum interference processes are destroyed when the energy levels of the two QDs are different from each other. As for the spin-down differential conductance $G_\downarrow$, it has a dip whose value can be suppressed to zero at $eV = 0$ due to the Fano antiresonance. The peaks of $G_\uparrow$ at other bias voltages are essentially the same as those of $G_\uparrow$ as the zero-energy modes of MBSs mainly change transport processes around the Fermi energy levels.

 doi:10.20944/preprints202506.1820.v1

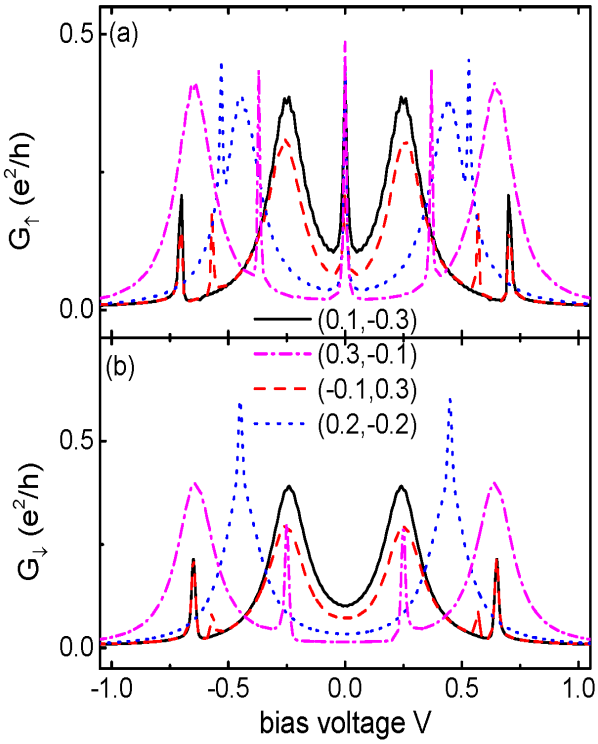

Figure 5. (a) $G_\uparrow$ and (b) $J_\downarrow$ as functions of the bias voltage V for different configurations of the dots' levels $\varepsilon_1, \varepsilon_2$ for $U = 1, \Gamma = 0.05, \lambda = 0.1$, and $T = 0$.

The two modes of the MBSs η_1 and η_2 couple to each other with strength of $\delta_M \sim e^{-L/\xi}$, where L is the length of the Majorana nanowire and ξ is the superconducting coherence length[32,36]. In Figure 6 we present functions of δ_M on the NDC in $G_\uparrow$ for different values of the system temperature T. It shows that if the nanowire is long enough so that $\delta_M \ll \lambda$, one can observe the NDC at low temperatures (see the black solid, red dashed and blue dotted lines). When the temperature is increased to 5×10^{-4} and 1×10^{-3}, $G_\uparrow$ becomes to be positive and the NDC disappears. The reason is that the impacts of the MBS are eliminated by thermal motion of the electrons at high temperatures. With increasing δ_M, $G_\uparrow$ first increases, reaching a maximum and then decreases to a constant value. The reason is that when the two modes of the MBSs overlap strongly with each other, they behave like the usual Dirac fermion. In fact, even the height of the ZBA in the differential conductance $G_\uparrow$ will also be changed in the presence of finite δ_M, and the signature of the MBSs disappears.

 doi:10.20944/preprints202506.1820.v1

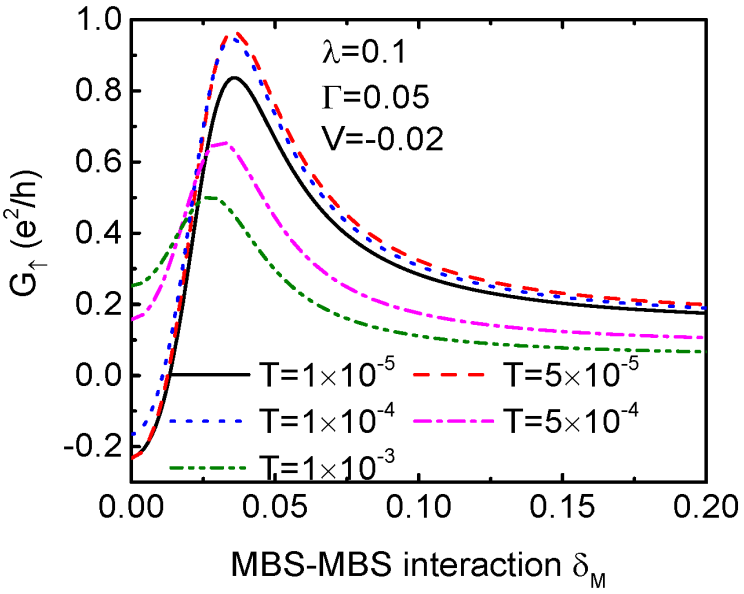

Figure 6. Dependence of $G_\uparrow$ at $V = -0.02$ around which NDC emerges on the MBS-MBS coupling strength δ_M for different system temperature T and indicated parameters. Other quantities are $U = 1$ and $t_c = 0.1$.

4. Summary

In summary, we have studied quantum transport through TDQDs with the side-coupled QD-2 is hybridized to a Majorana nanowire. It is found that due to the combined actions of the Coulomb interaction in the central QD-1 and the MBSs, the differential conductance of the spin-up electrons which couples to the MBSs is obviously changed. It can even be suppressed to negative value when the bias voltage is near to the zero-energy point, at which the differential conductance shows the well-known ZBA. This is the interesting NDC phenomenon unique in mesoscopic systems. The NDC is prone to occur under conditions of strong interdot coupling and low temperatures, and depends on the QD-MBS hybridization strength nonlinearly. The overlap between the MBSs will destroy the NDC and change the MBSs into usual Dirac fermion. The NDC as well as the ZBA in this TDQDs may serve as a reliable evidence of the existence of MBSs, and may also useful in designing particular mesoscopic electronic devices.

Author Contributions: Writing original draft preparation, Y.M. Gao, Y.F. Huang, F. Chi; writing review and editing, Y. F. Huang, Z.C. Yi, L.M. Liu and F. Chi. All authors have read and agreed to the published version of the manuscript.

Funding: This research was funded by the Education Science Planning Project of the Department of Education in Guang-dong Province (no. 2023GXJK542), the Educational Quality Project of the Department of Education in Guang-dong Province of China (no. SJD202302), the Graduate Joint Training Base (Zhongshan) Special Project in Guang-dong Province of China (no. 4YYJS04), Guangdong Province Education Department (Grant No. 2023KTSCX174), the Key Laboratory of Guangdong Higher Education Institutes (Grant No. 2023KSYS011), and Science and Technology Bureau of Zhongshan (Grant No. 2023B2035).

Institutional Review Board Statement: Not applicable.

Informed Consent Statement: Not applicable.

Data Availability Statement: All data included in this study are available upon request by contact with the corresponding author.

Conflicts of Interest: The authors declare no conflicts of interest.

 doi:10.20944/preprints202506.1820.v1

References

1. Read, N.; Green, D. Paired states of fermions in two dimensions with breaking of parity and time-reversal symmetries and the fractional quantum Hall effect. *Phys. Rev. B* **2000**, *61*, 10267. https://journals.aps.org/prb/abstract/10.1103/PhysRevB.61.10267.
2. Kitaev, A. Y. Unpaired Majorana fermions in quantum wires. *Phys.-Usp.* **2001**, *44*, 131. https://iopscience.iop.org/article/10.1070/1063-7869/44/10S/S29/meta
3. Qi, X.L.; Zhang, S.C. Topological insulators and superconductors. *Rev. Mod. Phys.* **2011**, *83*, 1057. https://doi.org/10.1103/RevModPhys.83.105
4. Alicea, J.; Oreg, Y.; Refael, G. Non-abelian statistics and topological quantum information processing in 1d wire networks. *Nat. Phys.* **2011**, *7*, 412. https://doi.org/10.1038/nphys1915.
5. Lian, B.; Sun, X.Q.; Vaezi, A.; Zhang, S.C. Topological quantum computation based on chiral Majorana fermions. *Proc. Natl. Acad. Sci.* **2018**, *115*, 10938. https://www.pnas.org/doi/full/10.1073/pnas.1810003115.
6. Mourik, V.; Zuo, K.; Frolov, S.M. Signatures of Majorana fermions in hybrid superconductor-semiconductor nanowire devices. *Science* **2012**, *336*, 1003. https://doi.org/10.1126/267science.1222360.
7. Deng, M.T.; Yu, C.L.; Huang, G.Y.; Larsson, M.; Caroff, P.; Xu, H.Q. Anomalous Zero-Bias Conductance Peak in a Nb-InSb Nanowire-Nb Hybrid Device. *Nano Lett.* **2012**, *12*, 6414. https://doi.org/10.1021/nl303758w.
8. Rokhinson, L.; Liu, X.; Furdyna, J. The fractional a.c. Josephson effect in a semiconductor-superconductor nanowire as a signature of Majorana particles. *Nature Phys* **2012**, *8*, 795. https://doi.org/10.1038/nphys2429.
9. Fu, L.; Kane, C.L. Superconducting Proximity Effect and Majorana Fermions at the Surface of a Topological Insulator. *Phys. Rev. Lett.* **2008**, *100*, 096407. https://journals.aps.org/prl/abstract/10.1103/PhysRevLett.100.096407.
10. Xu, J.P.; Wang, M.X.; Liu, Z.L. *et al*. Experimental detection of a Majorana mode in the core of a magnetic vortex inside a topological insulator-superconductor $Bi_2Te_3/NbSe_2$ heterostructure. *Phys. Rev. Lett.* **2015**, *114*, 017001. doi: 10.1103/PhysRevLett.114.017001.
11. Sau, J.D.; Lutchyn, R.M.; Tewari, S.; Das Sarma, S. Generic new platform for topological quantum computation using semiconductor heterostructures. *Phys. Rev. Lett.* **2010**, 104, 040502. doi: 10.1103/PhysRevLett.104.040502.
12. Hosur, P.; Ghaemi, P.; Mong, R.S.K.; Vishwanath, A. Majorana modes at the ends of superconductor vortices in doped topological insulators. **Phys. Rev. Lett. 2011**, *107*, 097001. doi: 10.1103/PhysRevLett.107.097001.
13. Wang, D.F.; Kong, L.Y.; Fan, P.; et al. Evidence for Majorana bound states in an iron-based superconductor. *Science* **2018**, *362*, 333. doi: 10.1126/science.aao1797.
14. Das Sarma, S.; Freedman, M.; Nayak, C. Topologically protected qubits from a possible non-Abelian fractional quantum Hall state. *Phys. Rev. Lett.*, **2005**, *94*, 166802. doi: 10.1103/PhysRevLett.94.166802.
15. Liu, T.T.; Wan, C.Y.; Yang, H. et al. Signatures of hybridization of multiple Majorana zero modes in a vortex. *Nature* **2024**, *633*, 71. https://doi.org/10.1038/s41586-024-07857-4.
16. Vaitiekenas, S.; Winkler, G.W.; van Heck, B. et al. Flux-induced topological superconductivity in full-shell nanowires. *Science* **2020**, *367*, 3392. DOI:10.1126/science.aav3392.
17. Pan, X.H.; Chen, L.; Liu, D.E.; Zhang, F.C.; Liu, X. Majorana Zero Modes Induced by the Meissner Effect at Small Magnetic Field. *Phys. Rev. Lett.* **2024**, *132*, 036602. https://journals.aps.org/prl/abstract/10.1103/PhysRevLett.132.036602.
18. Laroche, D.; Bouman, D.; van Woerkom, D.J. et al. Observation of the 4π-periodic Josephson effect in indium arsenide nanowires. *Nat. Commun.* **2019**, *10*, 245. https://doi.org/10.1038/s41467-018-08161-2 | www.nature.com/naturecommunications.
19. He, Q.L.; Pan, L.; Stern, A.L. et al. Chiral Majorana fermion modes in a quantum anomalous Hall insulator-superconductor structure. *Science* **2017**, *357*, 294. DOI:10.1126/science.aag2792.
20. Lopez, R.; Lee, M.; Serra, L.; Lim, J. Thermoelectrical detection of majorana states. *Phys. Rev. B* **2014**, *89*, 205418. https://doi.org/10.1103/PhysRevB.89.205418.
21. Chi, F.; Fu, Z.G.; Liu, J.; Li, K.; Wang, Z.; Zhang, P. Thermoelectric effect in a quantum dot side-coupled to majorana bound states. *Nanoscale Res. Lett.* **2020**, *15*, 79. https://doi.org/10.1186/s11671-020-03307-y.
22. Hong, L.; Chi, F.; Fu, Z.G.; Hou, Y.F.; Wang, Z. Large enhancement of thermoelectric effect by majorana bound states coupled to a quantum dot. *J. Appl. Phys.* **2020**, *127*, 124302. https://doi.org/10.1063/1.5125971.
23. Chi, F.; Liu, J.; Fu, Z.G. Yi, Z.C.; Liu, L.M. onlinear Seebeck and Peltier effects in a Majorana nanowire coupled to leads. *Chin. Phys. B.* **2024**, *33*, 077301. DOI: 10.1088/1674-1056/ad3f99.

 doi:10.20944/preprints202506.1820.v1

24. Klees, R.L.; Gresta, D.; Sturm, J.; Molenkamp, L.W.; Hankiewicz, E.M. Majorana-mediated thermoelectric transport in multiterminal junctions. *Phys. Rev. B* **2024**, *110*, 064517. https://journals.aps.org/prb/abstract/10.1103/PhysRevB.110.064517.
25. Chen, H.J.; Zhu, K.D. All-optical scheme for detecting the possible Majorana signature based on QD and nanomechanical resonator systems, *Sci. China Phys. Mech. Astron.* **2015**, *58* 050301. https://link.springer.com/article/10.1007/s11433-014-5637-4.
26. Tang, H.Z., Zhang, Y.T. and Liu, J.J. Photon-assisted tunneling through a topological superconductor with majorana bound states. *AIP Advances* **2015**, *5*, 127129. https://doi.org/10.1063/1.4939096.
27. Chi, F.; He, T.Y.; Wang, J.; Fu, Z.G.; Liu, L.M.; Liu, P.; Zhang, P. Photon-assisted transport through a quantum Dot side-coupled to majorana bound states. *Frontiers in Physics* **2020**, *8*, 00254.
28. Chi, F.; He, T.Y.; Zhou, G.F. Photon-Assisted Average Current Through a Quantum Dot Coupled to Majorana Bound States. *J. Nanoelectron. Optoelectron.* **2021**, *16*, 1325. DOI: https://doi.org/10.1166/jno.2021.3075.
29. Dmytruk, O.; Trif, M. Microwave detection of gliding Majorana zero modes in nanowires. *Phys. Rev. B* **2023**, *107*, 115418. https://journals.aps.org/prb/abstract/10.1103/PhysRevB.107.115418.
30. Pan, H.N.; Das Sarma, S. Physical mechanisms for zero-bias conductance peaks in Majorana nanowires. *Phys. Rev. Research* **2020**, *2*, 013377. https://journals.aps.org/prresearch/abstract/10.1103/PhysRevResearch.2.013377.
31. van der Wiel, W.G.; Franceschi, S.D. Elzerman, J.M.; Fujisawa, T.; Tarucha, S.; Kouwenhoven, L.P. Electron transport through double quantum dots. *Rev. Mod. Phys.* **2003**, *75*, 1. https://journals.aps.org/rmp/abstract/10.1103/RevModPhys.75.1.
32. Liu, D.E.; Baranger, H.U. Detecting a majorana-fermion zero mode using a quantum dot. *Phys. Rev. B* **2011**, *84*, 201308R. https://doi.org/10.1103/PhysRevB.84.201308.
33. Deng, M.T.; Vaitiekenas, S.; Hansen, E.B. et al. Majorana bound state in a coupled quantum-dot hybrid-nanowire system. *Science* 2016, 354, 1557. https://doi.org/10.1126/science.aaf3961.
34. Das Sarma, S. In search of Majorana. *Nat. Phys.* **2023**, *19*, 165. https://doi.org/10.1038/s41567-022-01900-9.
35. Yazdani, A.; von Oppen, F.; Halperin, B.I.; Yacoby, A. Hunting for Majoranas. *Science* **2023**, *380*, 0850. DOI:10.1126/science.ade0850
36. Prada, E.; Aguado, R.; San-Jose, P. Measuring Majorana nonlocality and spin structure with a quantum dot. *Phys. Rev. B* **2017**, *96*, 085418. https://doi.org/10.1103/PhysRevB.96.085418.
37. Zhao, H.J.; Wang, J.R.; Mao, H.; Jin, J.S. Distinguishing Majorana bound states from Andreev bound states through differential conductance and current noise spectrum. New Journal of Physics, Volume 27, February 2025
38. Gong, W.J.; Zhang, S.F.; Li, Z.C.; Yi, G.Y.; Zheng, Y.S. Detection of a Majorana-fermion zero mode by a T-shaped quantum-dot structure. *Phys. Rev. B* **2014**, *89*, 245413. https://doi.org/10.1103/PhysRevB.89.245413.
39. Ivanov, T.I. Coherent tunneling through a double quantum dot coupled to Majorana bound states. *Phys. Rev. B* **2017**, *96*, 035417. DOI: https://doi.org/10.1103/PhysRevB.96.035417
40. Majek, P.; Gorski, G.; Domanski, T.; Weymann, I. Hallmarks of Majorana mode leaking into a hybrid double quantum dot. *Phys. Rev. B* **2022**, *106*, 155123. DOI: https://doi.org/10.1103/PhysRevB.106.155123.
41. Aksenov, S.V. Probing Majorana bound states through an inhomogeneous Andreev double dot interferometer. *Phys. Rev. B* **2023**, *107*, 085417. DOI: https://doi.org/10.1103/PhysRevB.107.085417.
42. Pino, D.M.; Souto, R.S.; Aguado, R. Minimal Kitaev-transmon qubit based on double quantum dots. *Phys. Rev. B* **2024**, *109*, 075101. DOI: https://doi.org/10.1103/PhysRevB.109.075101
43. Murugan, B.; Lee, S.Y. Two-dimensional materials based on negative differential transconductance and negative differential resistance for the application of multi valued logic circuit: a review. *Carbon Letters* **2023**, *33*, 59. https://doi.org/10.1007/s42823-022-00423-w.
44. Fransson, J. Theory of current-voltage asymmetries in double quantum dots. *Phys. Rev. B* **2004**, *69*, 201304(R). https://journals.aps.org/prb/abstract/10.1103/PhysRevB.69.201304.
45. Chi, F.; Li, S.S. Current voltage characteristics in strongly correlated double quantum dots. *J. Appl. Phys.* **2005**, *97*, 123704. https://doi.org/10.1063/1.1939065.
46. Perrin, M.L.; Frisenda, R.; Koole, M. et al. Large negative differential conductance in single-molecule break junctions. *Nat. Nanotechnol.* **2014**, *9*, 830. DOI: 10.1038/NNANO.2014.177.
47. Wang, Y.; Zhang, Q.; Astier, H.P.A.G. et al. Dynamic molecular switches with hysteretic negative differential conductance emulating synaptic behaviour. *Nat. Mater.* **2022**, 21, 1403. https://doi.org/10.1038/s41563-022-01402-2.
48. Han, K.H.; Kim, S.H.; Kim, S.G. et al. Charge transfer mechanism for realization of double negative differential transconductance. *npj 2D Mater. Appl.* **2024**, *8*, 15. https://doi.org/10.1038/s41699-024-00454-z.

 doi:10.20944/preprints202506.1820.v1

49. Yang, K.H.; Guo, H.W.; Wang, H.Y.; Wei, Z.J.; Liang, X.H. Controllable antiresonance and low-bias negative differential conductance in T-shaped double dots with electron-phonon interaction. *Physica E: Low Dimens. Syst. Nanostruct.* **2024**, *163*, 116014. https://doi.org/10.1016/j.physe.2024.116014.
50. Cheng, S.G.; Sun, Q.F. Josephson current transport through T-shaped double quantum dots. *J. Phys. Condens. Matter* **2008**, *20*, 505202. https://doi.org/10.1088/0953-8984/20/50/505202.
51. Mathe, M.; Sticlet, D.; Zarbo, L.P. Quantum transport through a quantum dot side-coupled to a Majorana bound state pair in the presence of electron-phonon interaction. *Phys. Rev. B* **2022**, *105*, 155409. DOI: https://doi.org/10.1103/PhysRevB.105.155409.
52. Gao, Y.M.; Shen, Y.H.; Chi, F.; Yi, Z.C.; Liu, L.M. Quantum Transport through a Quantum Dot Coupled to Majorana Nanowire and Two Ferromagnets with Noncollinear Magnetizations. *Nanomaterials* **2024**, *14*, 1210. https://doi.org/10.3390/nano14141210.
53. Kumar, B.; Verma, S.; Ajay. Josephson and thermophase effect in interacting T-shaped double quantum dots system. *Physica E: Low Dimens. Syst. Nanostruct.* **2025**, 66, 116142. https://doi.org/10.1016/j.physe.2024.116142.
54. Calle, A.M.; Pacheco, M.; Martins, et al. Fano-Andreev effect in a T-shape double quantum dot in the Kondo regime. *J. Phys.: Condens. Matter* **2017**, *29*, 135301. doi:10.1088/1361-648X/aa58c1.